

**Amorphization by mechanical alloying in metallic systems with positive Gibbs energy of formation**Hai Yang Bai,<sup>1,2,\*</sup> C. Michaelsen,<sup>1</sup> C. Gente,<sup>1</sup> and R. Bormann<sup>1</sup><sup>1</sup>*Institute for Materials Research, GKSS-Research Center, Max-Planck Strasse, 21502, Geesthacht, Germany*<sup>2</sup>*Institute of Physics & Center for Condensed Matter Physics, Chinese Academy of Sciences, Beijing 100080, China*

(Received 7 August 2000; published 19 January 2001)

Fe-W has been chosen as a model system to investigate amorphization during mechanical alloying in systems with positive Gibbs energy of formation. Depending on the overall compositions, amorphous phases and supersaturated body-centered-cubic (bcc) Fe-W solid solutions were obtained by mechanical alloying. The thermodynamics of the system was determined by the calculation-of-phase-diagram (CALPHAD) method. The analysis shows that the Fe-W system exhibits a positive heat of mixing in the bcc solid solution, and a negative heat of mixing in the amorphous phase. As a result, the amorphous phase has a lower (however, still positive) Gibbs energy of formation than the solid solution in the concentration range of 17–42 at. % W, indicating that amorphization in this range is favored, in agreement with the experiments. The mechanism which allows amorphization and formation of solid solutions upon milling to occur in the Fe-W system is discussed. It is proposed that the elastic contribution to the excess enthalpy which originates from coherent interfaces between the elemental components provides a major driving force for alloying in the Fe-W system.

DOI: 10.1103/PhysRevB.63.064202

PACS number(s): 64.60.-i, 81.20.Ev, 81.05.Kf

**I. INTRODUCTION**

Mechanical alloying (MA) has been shown to be a versatile technique to produce metastable and unstable phases under highly nonequilibrium conditions, such as amorphous alloys, and supersaturated solid solutions frequently with grain sizes in the nanometer range.<sup>1</sup> Amorphization by MA has been investigated both experimentally and theoretically since the first discovery of amorphization by MA of elemental powder blends in the Ni-Nb binary system.<sup>2</sup> However, the studies of amorphization by MA have concentrated on transition-metal binary alloy systems exhibiting large negative heats of formation.<sup>3</sup> In such systems, easy formation of amorphous phases is obtained as a thermodynamic driving force for amorphization and favorable kinetics with large interdiffusion coefficients exist.

More recently, amorphization by MA has also been observed in systems exhibiting positive Gibbs energy of formation, e.g., Cu-*M* (*M*=Ta, W, Ag, and Cr),<sup>4–7</sup> Fe-W,<sup>8,9</sup> and several explanations for the thermodynamically unexpected formation of the amorphous phase have been proposed. For the Cu-Ta system, which is immiscible in the solid state, it has been suggested that the amorphization is due to refinement of grains by MA.<sup>4,10,11</sup> Alloying occurs until the average grain size of Cu and Ta crystallites is reduced to about 10 nm and, once it reaches this level, the increase in interfacial energy of grain boundaries was proposed to be large enough to allow the formation of an amorphous phase. The Cu-W system is an immiscible system both in the solid and liquid states, and exhibits a very large positive heat of mixing for solid solutions.<sup>5,12,13</sup> Depending on milling conditions, mechanical alloying of elemental powder blends either results in partial amorphization<sup>5</sup> or supersaturated solid solutions.<sup>12</sup> As a mechanism for alloy formation, it was proposed that large lattice expansion and grain refinement result in a destabilization of the crystalline lattice. The results obtained in the Cu-Ta and Cu-W systems raise the question on the influence of impurities which can originate from the mill-

ing atmosphere as well as from abrasion of vials and milling balls. For instance, in the case of Cu-W, steel vials and balls were used. However, no impurity analysis has been reported in the investigations. The MA in the Cu-Ta system was carried out by using Cu(Be) vial and balls. Thus, chances to be contaminated by Fe are fully absent. But interstitial atoms such as oxygen and nitrogen also might favor amorphization. In the Cu-Ag system, which has a heat of mixing of 9 kJ/g atom for the bcc solid solution,<sup>6</sup> the amorphous phase was formed during milling in Ar. No amorphization occurred upon milling in air. Contamination of the metal powder by oxygen affects both the time required to achieve the amorphous phase and its crystallization.<sup>6</sup> In contrast to the Cu-Ag system, both fcc and bcc solid solutions were formed by MA under argon atmosphere in the Cu-Cr system which exhibits a positive enthalpy of mixing up to about 20 kJ/g atom (at about 400–500 °C).<sup>7</sup> The nanocrystalline Cu-Cr solid solutions transformed to an amorphous phase when Cr-rich alloys were additionally milled in atmospheres containing oxygen or nitrogen. It was supposed that oxygen and nitrogen promote the grain refinement and cause the amorphization.<sup>7</sup> Amorphization has also been observed in the Fe-W system.<sup>8,9</sup> Partial amorphization and nanocrystalline solid solutions were achieved already by milling pure W powder. However, because of the hardness of W, contamination and alloying with Fe by abrasion from the milling tools occurred.<sup>8</sup> The mechanism of amorphous phase formation was therefore mainly attributed to Fe and Cr contamination. X-ray diffraction analysis shows that the crystallite strain increased with milling time till amorphization occurred and decreased subsequently. Correlating the stored energy with the microstrain, the crystallite strain was proposed to provide driving force necessary for the formation of the amorphous phase.<sup>8</sup> Milling of an equiatomic mixture of the elemental Fe and W powers, only a small amount of amorphous phase together with W-rich bcc solid solution formed.<sup>9</sup> The large stored energy of about 10 kJ/g atom was interpreted to result from the increased solution of W in Fe and the refinement of grain size, leading to a destabilization of the crystalline phase and a partial transformation into the amorphous phase.

TABLE I. Compositions of the Fe-W powders under different conditions measured by EDX (for the Fe, W, and Cr contents) and chemical analysis (for the oxygen and nitrogen contents). Dashes indicate Cr content is below detection limit.

Powders with starting compositions	Milling time (h)	Fe (at. %)	W (at. %)	Cr (at. %)	O (wt. %)	N (wt. %)
Fe <sub>80</sub> W <sub>20</sub>	0				0.14	
	200				0.16	0.042
	1400	80.49	19.51	-	0.23	0.19
Fe <sub>70</sub> W <sub>30</sub>	200	69.65	30.35	-		
	600	71.50	27.12	1.38		
	1400	72.55	25.64	1.81		
	2000	75.44	21.99	2.57		
Fe <sub>50</sub> W <sub>50</sub>	0	50.53	49.47	-	0.073	
	50	48.29	51.71	-		
	100	53.64	45.48	0.87		
	200	70.46	26.93	2.62	0.073	0.026
	1400	76.40	18.31	5.28	0.081	0.15
	2000	78.54	15.99	5.47		
	200 <sup>a</sup>				0.089	0.028
Fe <sub>20</sub> W <sub>80</sub>	0				0.04	
	200	20.64	79.36	-	0.093	0.037
	600				0.16	0.14
	1400	20.21	79.21	-		

<sup>a</sup>The sample milled for 200 h was exposed to air for 7 months.

The thermodynamic functions of the Fe-W system were calculated in Ref. 9 using Miedema's semiempirical model. However, the calculation showed that the Gibbs energy of the amorphous phase is larger than that of the bcc phase over entire concentration range. Thus the thermodynamic analysis could not explain the experimental results.

To conclude, in previous investigations the mechanism of amorphization is mainly attributed to a decrease of the grain size of the pure elements upon milling. The excess enthalpy is suggested to be stored in the grain boundaries, and the interfacial energy of the grain boundaries is proposed to provide the driving force for amorphization. However, on the other hand, in earlier work, it was concluded that the excess enthalpy stored in grain boundaries is insufficient to act as a driving force for the formation of either a solid solution with enhanced solubility or an amorphous phase if alloy exhibits a positive Gibbs energy of formation larger than 1–2 kJ/g atom.<sup>14</sup> Impurities are also suspected to affect alloying in systems with positive heats of mixing. In Ref. 6 oxygen was unfavorable for amorphization, in Ref. 7 the impurities resulted in amorphization. In Refs. 15 and 16 impurities were suspected to decrease the heat of mixing.

In the present work, the Fe-W binary system has been chosen as a model system to investigate the mechanisms of amorphization during MA in systems with positive Gibbs energy of formation. The Fe-W alloys with different compositions are produced by mechanical alloying, and the thermodynamics of the Fe-W system is determined by the CALPHAD method. Based on our results, a mechanism of the phase formation during MA is proposed based on the

elastic energy of coherent interfaces between the elemental components.

## II. EXPERIMENT

Milling was performed with a planetary mill (Fritsch Pulverisette 5) with hardened steel vials and balls. All handling of the powders including the milling procedure was performed in a glove box under purified argon. Oxygen and water contents of the atmosphere during milling were kept below 1 ppm. The process was interrupted each 15 min for 15 min to cool down the vials which heated up typically to about 50 °C during milling. The ball-to-powder weight ratio was 10:1. The purity of the Fe powder was 99.5 wt. % (0.23 wt. % O), with a particle size less than 45 μm. The purity of the W powder was 99.95 wt. % (0.03 wt. % O), with a particle size 4–5 μm. The elemental Fe and W powder blends were prepared with nominal compositions of 20, 30, 50, and 80 at. % W. The mixtures of the powders were milled up to 2000 h. The structural evolution during mechanical alloying and subsequent annealing was investigated by x-ray diffraction (XRD) using Cu K<sub>α</sub> radiation. Differential scanning calorimetry (DSC) was carried out with a calibrated high-temperature calorimeter of type Netsch DSC 404. Additional Fe pickup from the vials and balls was determined by energy-dispersive x-ray (EDX) analysis in a scanning electron microscope. The oxygen and nitrogen contents of the initial powder blends and the milled powders were determined by chemical analysis. The results are summarized in Table I. It can be seen that the oxygen content even after long time milling is increased only slightly, but stays typi-

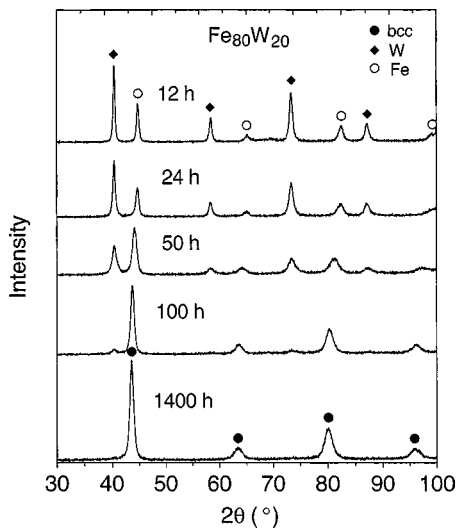


FIG. 1. XRD patterns of as-mixed and milled  $\text{Fe}_{80}\text{W}_{20}$  powder for selected milling times.

cally below 0.23 wt. %. After exposure to air for 7 months, the O and N contents are almost unchanged, see for example in case of  $\text{Fe}_{50}\text{W}_{50}$  in Table I. The relatively small increase in the oxygen and nitrogen contents during milling, and after exposure to air, demonstrates that the Fe-W alloys do not rapidly react with oxygen and nitrogen.

No significant Fe abrasion from vials and balls occurred in the  $\text{Fe}_{80}\text{W}_{20}$ , and  $\text{Fe}_{20}\text{W}_{80}$  powders even after 1400 h milling. However, some Fe abrasion occurred in the  $\text{Fe}_{70}\text{W}_{30}$  powder (original composition), changing the composition to 75.4 at. % Fe, 22.0 at. % W, and 2.6 at. % Cr after 2000 h milling. A large amount of Fe abrasion took place in the  $\text{Fe}_{50}\text{W}_{50}$  powder (original composition) during milling. As shown in Table I, the composition of the  $\text{Fe}_{50}\text{W}_{50}$  powder changed to 78.5 at. % Fe, 16.0 at. % W, and 5.5 at. % Cr after 2000 h milling. For convenience, in the remainder of the text, figures and their accompanying captions, the powders are cited by their original (nominal) compositions, i.e.,  $\text{Fe}_{80}\text{W}_{20}$ ,  $\text{Fe}_{70}\text{W}_{30}$ ,  $\text{Fe}_{50}\text{W}_{50}$ , and  $\text{Fe}_{20}\text{W}_{80}$ . Real compositions can be obtained by referring to Table I.

### III. RESULTS

#### A. Mechanical alloying of the $\text{Fe}_{80}\text{W}_{20}$ powder blends

Figure 1 shows XRD patterns of the milled  $\text{Fe}_{80}\text{W}_{20}$  powder for selected milling times. For increasing milling time, the positions of the W peaks remain unchanged, but their intensities decrease upon milling while the Fe peaks shift to lower angles. After 1400 h milling, the W peaks completely vanished, the intensities and the positions of the Fe peaks do not change any more, indicating the formation of a Fe-rich solid solution. The grain size of the  $\text{Fe}_{80}\text{W}_{20}$  powder is reduced to about 17 nm after 1400 h milling as derived from the width of the diffraction peaks by method of Williamson and Hall.<sup>17</sup> These results indicate that W was dissolved into the Fe. Little contamination took place during this process.

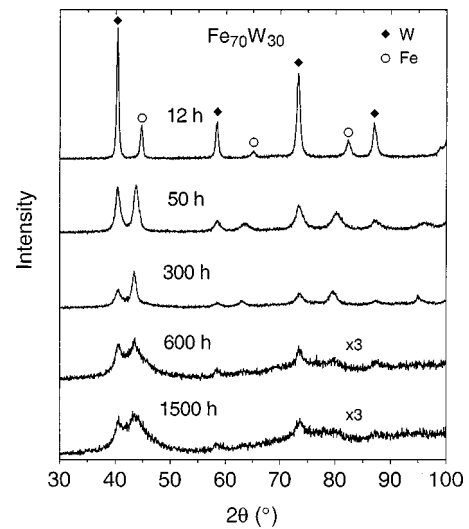


FIG. 2. XRD patterns of milled  $\text{Fe}_{80}\text{W}_{20}$  powder for selected milling times.

#### B. Mechanical alloying of the $\text{Fe}_{70}\text{W}_{30}$ powder blend

Figure 2 shows XRD patterns of the milled  $\text{Fe}_{70}\text{W}_{30}$  powder for selected milling times. At the early stage of milling, both Fe and W peaks do not shift, but the intensities decrease and the peaks are broadened. After 50 h of milling the Fe peaks shift to lower angles, indicating the formation of a Fe-rich solid solution. The positions of the W peaks do not change upon milling, but the peaks are broadened and weakened. After 600 h milling, an amorphous phase is formed on the expense of W and the Fe-rich bcc solid solution. A large part of the amorphous phase forms after 1500 h milling. The abrasion occurs during this process. From Table I and Fig. 2 it is noticed that the transformation to the amorphous phase occurred before the abrasion started, at milling time of about 600 h. It is supposed that the Fe abrasion is due to the mechanical property of the powder, i.e., hardness of the amorphous phase.

#### C. Mechanical alloying of the $\text{Fe}_{50}\text{W}_{50}$ powder blend

Figure 3 shows XRD patterns of the mechanically alloyed  $\text{Fe}_{50}\text{W}_{50}$  powder. For milling time less than 50 h, the milling product is a mixture of W and Fe-rich solid solutions. The positions of the W peaks do not change upon milling, but the peaks are broadened and weakened. The Fe peaks shift to lower angles, rapidly weakened and broadened. After 100 h milling, an amorphous phase is formed on the expense of W and the Fe-rich bcc solid solution. Afterwards the situation is similar to the  $\text{Fe}_{70}\text{W}_{30}$  powder, but the onset time for amorphization is much earlier than that for the  $\text{Fe}_{70}\text{W}_{30}$  powder. Amorphization in this sample occurs only after 100 h milling. An almost completely amorphous phase forms after 1500 h milling. The abrasion also occurs during this process. From Table I and Fig. 3 it is noticed again that the transformation to the amorphous phase occurred before the abrasion started, at milling time of about 100 h. The Cr content due to abrasion is 0.87 at. % after 100 h milling. However, it is also not considered as the reason of the amorphization in the Fe-W system.

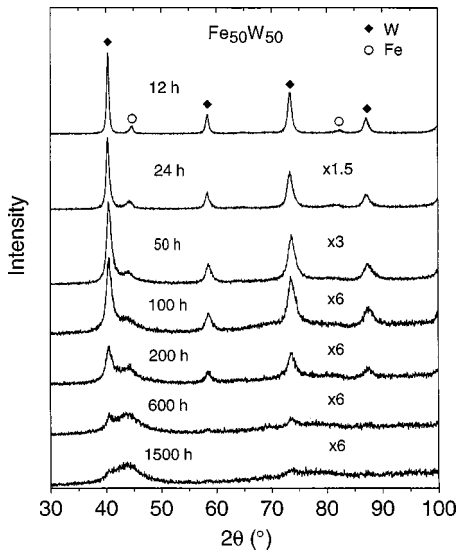


FIG. 3. XRD patterns of milled  $\text{Fe}_{50}\text{W}_{50}$  powder for selected milling times.

**D. Mechanical alloying of the  $\text{Fe}_{20}\text{W}_{80}$  powder blend**

Figure 4 shows XRD patterns of the as-mixed and mechanically alloyed  $\text{Fe}_{20}\text{W}_{80}$  powder for selected milling times. It can be seen that the intensities of the Fe peaks decrease rapidly upon milling and disappear after 50 h milling. The W peaks are broadened due to reduction of grain size and increase in internal strain. In addition, the Fe peaks shift to higher diffraction angles upon milling time indicative of some dissolution of Fe into the W. No observable change takes place in peak positions and widths of the XRD patterns after 200 h milling. This suggests that a bcc W-rich solid solution is formed after 200 h milling. The lattice parameter of the W-rich solid solution decreases from 0.3165 nm to 0.3123 nm as derived from the shift of x-ray diffraction peaks, and the grain size of the solid solution is reduced to about 20 nm as derived from the width of the diffraction peaks by the method of Williamson and Hall.<sup>17</sup> These results indicate that Fe was dissolved into the W. Comparison of the

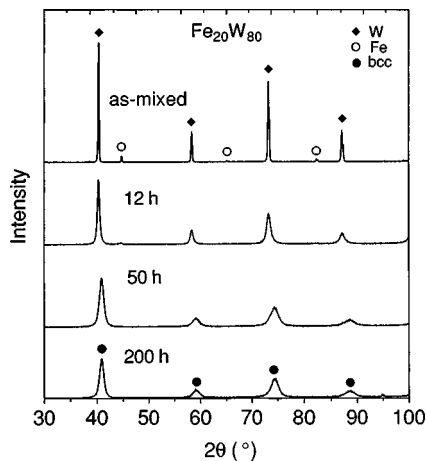


FIG. 4. XRD patterns of milled  $\text{Fe}_{20}\text{W}_{80}$  powder for selected milling times.

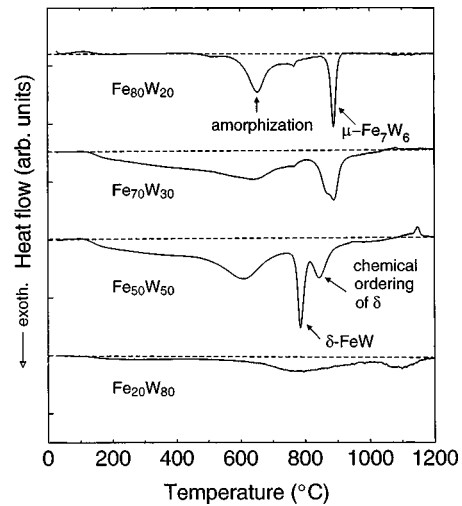


FIG. 5. DSC traces of the Fe-W powders with different compositions after mechanical alloying for 600 h.

milling time required to form the W-rich solid solution (200 h) and the Fe-rich solid solution (1400 h) shows that the formation of a W-rich solid solution is significantly faster than the formation of a Fe-rich solid solution. Little Fe abrasion took place in this process and it is considered as it is due to the softness of the Fe-W solid solution powders (the milled  $\text{Fe}_{80}\text{W}_{20}$  and the  $\text{Fe}_{20}\text{W}_{80}$ ), which can be felt by hands. In addition, the particles of the Fe-W solid solution powders look fine, but the particles that with amorphous phase are coarse (the milled  $\text{Fe}_{70}\text{W}_{30}$  and the  $\text{Fe}_{50}\text{W}_{50}$ ).

**E. Heat treatment of the mechanically alloyed Fe-W samples**

The mechanically alloyed Fe-W powders were investigated by DSC, in combination with subsequent x-ray diffraction analysis. All DSC measurements were carried out at a constant heating rate of 20 K/min. DSC traces of the mechanically alloyed  $\text{Fe}_{80}\text{W}_{20}$ ,  $\text{Fe}_{70}\text{W}_{30}$ ,  $\text{Fe}_{50}\text{W}_{50}$ , and  $\text{Fe}_{20}\text{W}_{80}$  powders milled for 600 h are displayed in Fig. 5.

The DSC trace of the  $\text{Fe}_{80}\text{W}_{20}$  sample exhibits two major exothermic peaks at approximately 650 °C and 885 °C (Fig. 5). The corresponding XRD pattern (Fig. 6) shows that the bcc solid solution decomposes into an amorphous phase and a Fe-rich solid solution upon heating to 740 °C, and then crystallizes into the  $\mu\text{-Fe}_7\text{W}_6$  at 885 °C (Fig. 6). A support for the presence of an amorphous phase was provided by the investigation of the transformation behavior towards equilibrium in the DSC measurements, which showed that this transformation takes place in a rather narrow temperature range, a feature that is characteristic of crystallization of an amorphous phase, or characteristic of usual nucleation-and-growth processes in general. In another work we showed that inverse melting in the Fe-W system, which demonstrated a polymorphous transformation from the solid solution to a complete amorphous phase with the compositions of  $\text{Fe}_{70}\text{W}_{30}$  and  $\text{Fe}_{67}\text{W}_{33}$  by cosputtering and annealing.<sup>18</sup> For further conformation TEM observation is needed. The small exothermic peak at 767 °C results from the baseline and corresponds to the magnetic transformation of Fe in the baseline

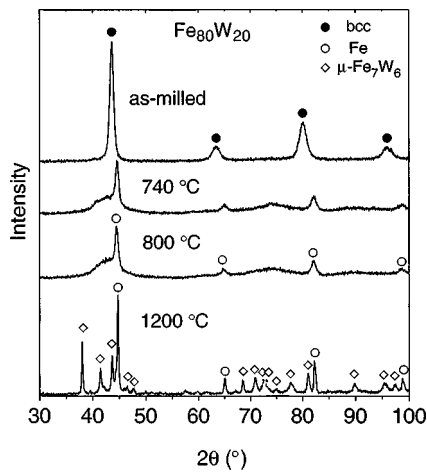


FIG. 6. XRD patterns of milled Fe<sub>20</sub>W<sub>80</sub> powder after heating to selected temperatures.

run. (The Curie temperature  $T_c$  of pure Fe is 770 °C,<sup>19</sup> and is not markedly affected by the W content.<sup>20,21</sup>)

Figure 7 gives XRD patterns of the milled and heated Fe<sub>70</sub>W<sub>30</sub> powder. The DSC scan and the XRD patterns of the Fe<sub>70</sub>W<sub>30</sub> powder show that during heating up to 1200 °C the amorphous phase first structurally relaxes, subsequently Fe is precipitated and finally the μ-Fe<sub>7</sub>W<sub>6</sub> phase is formed.

As shown in Fig. 5, the DSC trace of the Fe<sub>50</sub>W<sub>50</sub> specimen exhibits three exothermic peaks at approximately 610 °C, 775 °C, and 840 °C, respectively. Figure 8 shows XRD patterns of the milled Fe<sub>50</sub>W<sub>50</sub> powder after heating to selected temperatures. During heating up to 700 °C (over the first broad exothermic peak), the amorphous phase structurally relaxes and partially decomposes to Fe and W-rich solid solution. The formation of the δ-FeW compound and precipitation of Fe occur upon heating to 770 °C, and this process continues upon heating to 800 °C. The third peak is related to chemical ordering of δ-phase. The formation of δ-phase instead of μ-phase in the Fe<sub>50</sub>W<sub>50</sub> powder is likely due to the high Cr content in the Fe<sub>50</sub>W<sub>50</sub> powder. The enthalpies associated with the second and the third peaks are 2.8 and 2.1

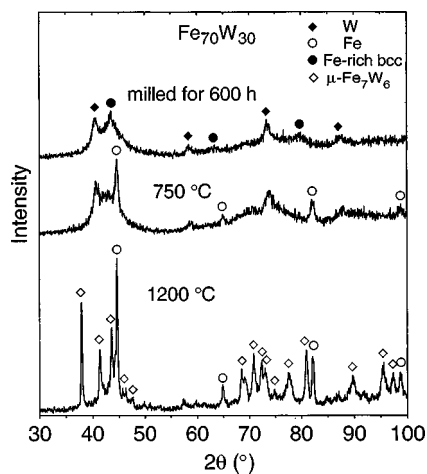


FIG. 7. XRD patterns of milled Fe<sub>50</sub>W<sub>50</sub> powder after heating to selected temperatures.

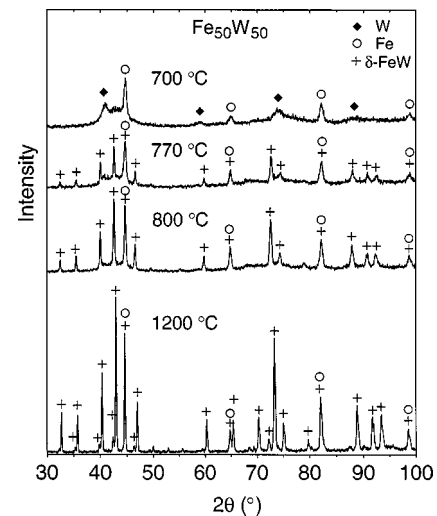


FIG. 8. XRD patterns of milled and heated Fe<sub>70</sub>W<sub>30</sub> powder.

kJ/g atom, respectively. These enthalpy values are important for the thermodynamic calculations of the Fe-W system.

The Fe<sub>20</sub>W<sub>80</sub> sample displays two broad exothermic heat releases in the DSC scan between room temperature and 1200 °C. Integration of the signal gives the values of 5.5 and 1.6 kJ/g atom for the first and the second broad peaks, respectively. Figure 9 shows XRD patterns of the milled Fe<sub>20</sub>W<sub>80</sub> powder after heating to selected temperatures in the DSC. XRD of a sample heated up to the end of the first broad peak (950 °C) shows that the peaks of the W-rich solid solution shift to lower angles and become narrow and sharp, indicating the precipitation of Fe (or Fe-rich solid solution) from the W-rich solid solution and the grain growth during this process. Since the amount of precipitant Fe and its grain size are small, the Fe peaks cannot be detected in the XRD pattern. Furthermore, the heat release of the first peak (5.5 kJ/g atom) is too large for the relaxation and grain growth, so it can be concluded that around 800 °C the supersaturated

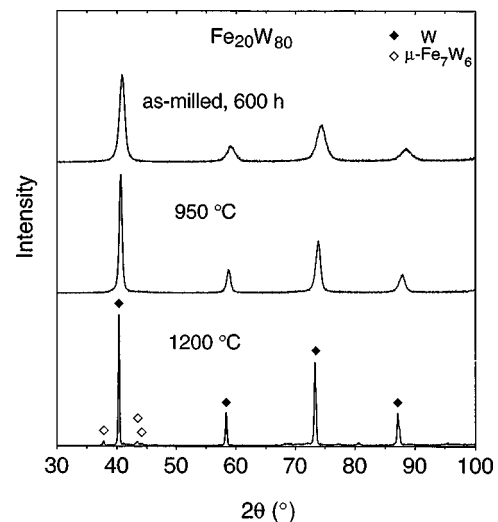


FIG. 9. XRD patterns of the Fe<sub>80</sub>W<sub>20</sub> powder after heating to different temperatures. The bcc solid solution decomposed into an amorphous phase and Fe at 740 °C and 800 °C.

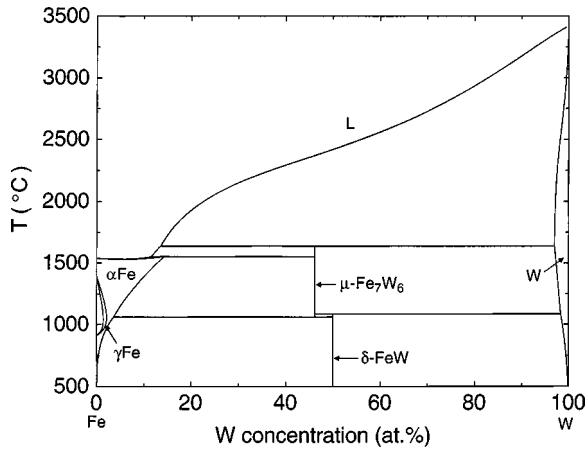


FIG. 10. Phase diagram of the Fe-W system calculated by the CALPHAD method.

solution decomposes into a W-richer and a Fe-richer solutions. The equilibrium compound  $\mu\text{-Fe}_7\text{W}_6$  forms during the second exothermal process, and the enthalpy of reaction amounts to 1.6 kJ/g atom.

**F. The CALPHAD calculation results**

The thermodynamic functions of the Fe-W system are determined by the CALPHAD method. The calculations are based on data of the equilibrium phase diagram, available thermodynamic data from the literature, and the heats of transformation determined in this work by DSC. The magnetic contributions are also considered in present evaluation.

Figure 10 represents the calculated equilibrium phase diagram of the Fe-W system. Figure 11 shows an interesting phenomenon of the Fe-W system: the heats of mixing of the liquid phase change their sign from positive to negative as a function of temperature. This phenomenon was first discovered in the immiscible Nb-Cu system,<sup>22</sup> and is explained in terms of the tight binding model of the electron theory. The change of the sign of the heats of mixing of the liquid directly relates to the negative heat of mixing of the amorphous phase, since the amorphous phase is taken as the undercooled liquid phase below the glass transition. Figure 12 shows the enthalpies for the corresponding phases at 300 °C. Modeling of the milling process shows that depending on the

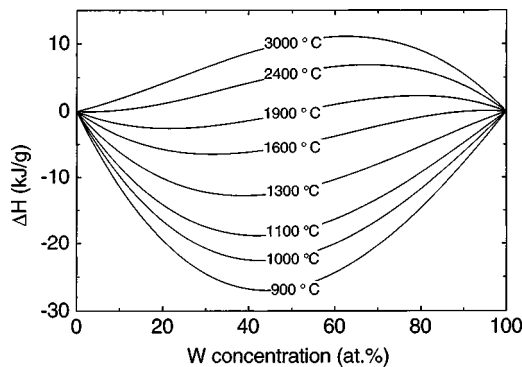


FIG. 11. Heats of mixing of the liquid phase at different temperatures, calculated by the CALPHAD method.

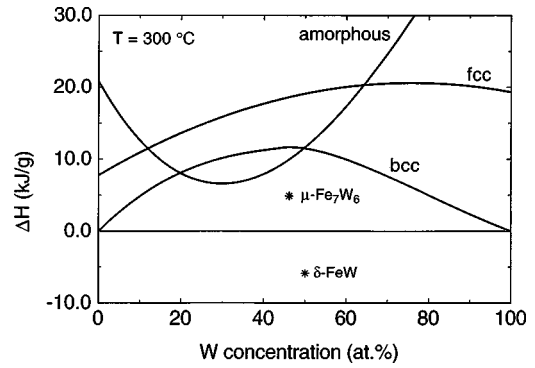


FIG. 12. The enthalpies of the metastable and the stable phases of the Fe-W system at  $T=300\text{ }^\circ\text{C}$ . The bcc phase is taken as enthalpy reference state.

milling conditions and on the properties of the powder the temperature rise at interfaces of powder particles during the collision process can amount up to several hundred degrees. Thereby, interdiffusion can occur at the interface, if a driving force for a reaction exists. For the Fe-W composite,  $T=300\text{ }^\circ\text{C}$  is considered as a typical interface temperature during ball milling. Figure 12 demonstrates that the Fe-W system exhibits a positive heat of mixing for the bcc solid solution with a maximum value of +11.7 kJ/g atom at the concentration of 46 at. % W, and +11.5 kJ/g atom at the equiatomic concentration. Figure 13 shows the Gibbs energy curves of the bcc and the fcc solid solutions, the amorphous phase,  $\mu\text{-Fe}_7\text{W}_6$  and  $\delta\text{-FeW}$  compounds at the same temperature (300 °C). The Fe-W system exhibits a positive Gibbs energy of formation for the amorphous phase with a minimum value of 4.1 kJ/g atom at the concentration of 24 at. % W. Figure 13 indicates that there is no thermodynamic driving force to form either a concentrated solid solution or an amorphous phase from the elemental components. At 300 °C, the Gibbs energy curves of the bcc and the amorphous phases intersect at the concentrations of 17 and 42 at. % W. In this concentration range the Gibbs energy of the amorphous phase is lower than that of the bcc phase, i.e., the amorphous phase is energetically preferred over the bcc

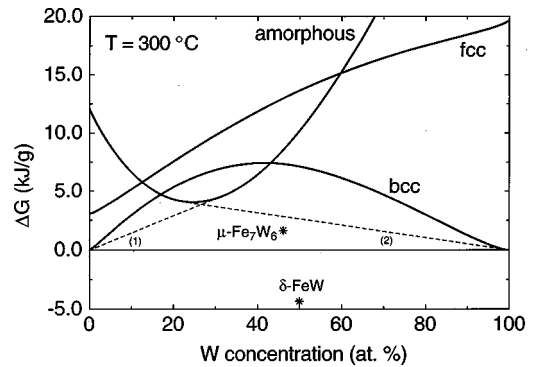


FIG. 13. The Gibbs energies of the metastable and the stable phases in the Fe-W system at  $T=300\text{ }^\circ\text{C}$ . The bcc phase is taken as Gibbs energy reference state. The dashed lines (1) and (2) are common tangents between the amorphous phase and the Fe-rich or W-rich bcc solid solution, respectively.

phase. However, the maximum difference of Gibbs energies between the two phases only amounts to about 2.4 kJ/g atom. This may explain why in the Fe-W system it is not easy to get a single amorphous phase. Usually the amorphous phase and the bcc phase coexist in milled powders within this concentration range.

#### IV. DISCUSSION

From the results' section it is summarized that amorphous phase and solid solutions form by MA although these phases exhibit positive Gibbs energy of formation, and therefore no driving force for alloying exists from the elemental components. So the results should be discussed by the combination of the thermodynamics of the system and the mechanisms of MA.

##### A. Thermodynamics of the Fe-W system

From the equilibrium phase diagram and the CALPHAD results, an equilibrium compound,  $\delta$ -FeW exists which exhibits a negative (however small) heat of formation ( $-6.4$  kJ/g atom). This indicates that Fe and W atoms are slightly attractive, since the heat of formation of the compound mainly originates from a chemical contribution ( $\Delta H_{\text{chem}}$ ) to the enthalpy. This result is in agreement with a simple electron band model, which predicts the heats of formation for the transition metal alloys at equiatomic composition.<sup>23,24</sup> As the total enthalpy of mixing is the sum of a chemical and a structural contribution, i.e.,  $\Delta H = \Delta H_{\text{chem}} + \Delta H_{\text{str}}$ , the positive heat of mixing for the bcc solid solution in the Fe-W system originates mainly from the structural contribution ( $\Delta H_{\text{str}}$ ). Due to the large atomic size mismatch ( $\Delta r/r = 9.8\%$ ),  $\Delta H_{\text{str}}$  is mainly determined by the elastic enthalpy, i.e.,  $\Delta H_{\text{str}} = \Delta H_{\text{el}}$ . Therefore  $\Delta H_{\text{str}}$  for solid solution can be estimated by classical elasticity theory using the "sphere and hole" model, and an expression for the elastic enthalpy per mole of solute metal  $A$  in matrix metal  $B$  is given by<sup>25,26</sup>

$$\Delta H_{\text{el}}(A \text{ in } B) = \frac{2K_A\mu_B(V_B - V_A)^2}{3K_A V_B + 4\mu_B V_A}, \quad (1)$$

where  $\mu_B$  is the shear modulus of the host,  $K_A$  the bulk modulus of the solute metal,  $V_A$  and  $V_B$  are the molar volumes of  $A$  and  $B$  atoms considering the correction for charge transfer effect. If the molar fractions of solute and solvent metal are included, the elastic enthalpy is expressed by

$$\Delta H_{\text{el}} = X_A X_B [X_B \Delta H_{\text{el}}(A \text{ in } B) + X_A \Delta H_{\text{el}}(B \text{ in } A)], \quad (2)$$

where  $X_A$  and  $X_B$  are the atomic fractions of components  $A$  and  $B$  in the alloy. Thus the elastic contribution to  $\Delta H_{\text{str}}$  due to the atomic mismatch in the equiatomic solid solution is derived to be 9.0 kJ/g atom without considering the temperature effect on the modulus to the  $\Delta H_{\text{str}}$ . Therefore we will assume as a reasonable approximation that  $\Delta H_{\text{chem}}$  is about 2.5 kJ/g atom and  $\Delta H_{\text{str}}$  amounts to 9.0 kJ/g atom, since  $\Delta H = 11.5$  kJ/g atom for the equiatomic composition in the Fe-W systems.

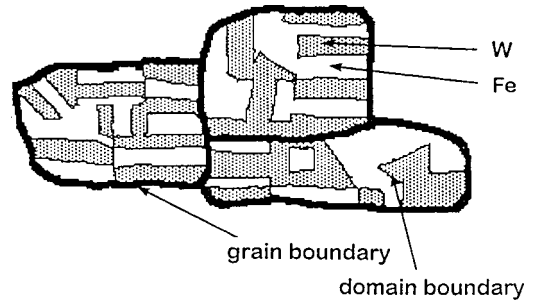


FIG. 14. Schematic diagram of the grains and domains in milled Fe-W powder.

##### B. The mechanism of phase formation by mechanical alloying in the Fe-W system

The maximum equilibrium solid solubility of Fe in W is 2.6 at. % Fe at 1637 °C, and it is below 1 at. % at 500 °C.<sup>21</sup> In contrast, the solid solubility was extended by mechanical alloying to at least 20 at. % W in Fe, and Fe in W. This corresponds to an increase in the Gibbs energy of 5.3 kJ/g atom and 3.0 kJ/g atom at  $T = 300$  °C, respectively. How these energies are stored in a system before alloying occurs is an important aspect of the mechanism of MA. In previous work it was explained by grain refinement during milling. The energy stored in grain boundaries was suggested to provide the main driving force for the formation of supersaturated solid solutions.

In the Fe-W system, the typical grain size after long milling times is about 20 nm. The enthalpy stored in the grain boundaries can be estimated by assuming a cubic grain size and using the formula  $\Delta H_g = 3\sigma_g \bar{V}_m / D$ .  $\sigma_g$  is the interfacial energy of the grain boundaries of the elemental Fe and W crystallites which we estimate to be 0.5–1.0 J/m<sup>2</sup>.  $\bar{V}_m$  is the average molar volume, and  $D$  is the grain size. Using these values, an excess enthalpy of 0.6–1.3 kJ/g atom is obtained. This demonstrates that the excess enthalpy stored in the grain boundaries is far from enough to provide the driving force for the formation of the Fe-W solid solution and the amorphous phase.

Therefore, we propose here a new model for alloy formation by MA in the Fe-W system, which is based on the model of coherent composites developed by Gente *et al.*,<sup>14</sup> however considers the elastic contribution of the atomic size mismatch as discussed above. In this model, it is proposed that coherent interfaces between Fe and W components form upon continuous deformation by milling, and an elastic contribution to the enthalpy arises from the coherent interfaces due to the large atomic size mismatch. The interfacial chemical energy and the elastic energy at the domain boundaries should provide the driving force for the formation of Fe-W solid solutions and amorphous phases. We suggest that during milling grains (of typical size of 20 nm) are formed which consist of very small coherent Fe and W elemental regions (Fig. 14). This implies that the composition in a grain is not homogeneous. These small elemental regions are termed domains.<sup>14,27</sup> Such coherent elemental domains are frequently observed in multilayer films, when the interfaces are coherent so that the grain sizes are larger than the layer

thickness. Examples are Cu/Co<sup>27</sup> and also Fe/W<sup>28</sup> multilayer films. Using Mössbauer spectroscopy, chemically heterogeneous zones, with unalloyed Fe and W, were indeed deduced to persist during mechanical alloying of ball milled Fe<sub>50</sub>W<sub>50</sub>.<sup>29</sup> Furthermore, the direct experimental evidence for the occurrence of such elemental domains within the grains of the milled Cu-Co powder blends has also been presented recently.<sup>30</sup> The Gibbs energy of such chemically inhomogeneous (composite) grains consists of two contributions: first, the chemical contribution related to difference in concentration across the coherent interfaces,

$$\Delta H_{\text{chem}}^{\text{comp}} = S \sigma_{\text{chem}}, \quad (3)$$

where  $S$  is the interface area of per gram atom composite and  $\sigma_{\text{chem}}$  the interface energy (per unit area), and secondly the structural (elastic) contribution which originates from atomic mismatch across the interfaces,

$$\Delta H_{\text{el}} = \frac{1}{2} E \epsilon^2 \bar{V}_m, \quad (4)$$

where  $E$  is the Young's modulus of elasticity,  $\epsilon$  is the strain that originates from atomic mismatch across the interfaces, and  $\bar{V}_m$  is the average molar volume.

The chemical contribution of the interface Gibbs energy,  $\sigma_{\text{chem}}$ , can be calculated for systems with positive heats of mixing by using a simple pair interaction model developed by Becker.<sup>31</sup> By neglecting entropy contributions, the interface energy thus scales with the square of the concentration difference across the interface,  $\Delta c$ , and the pair exchange energy  $\Omega$ , which is positive in systems with positive heats of mixing:

$$\sigma_{\text{chem}} = n_s Z_s \Omega \Delta c^2, \quad (5)$$

where  $n_s$  is number of atoms per unit area at the domain boundary and  $Z_s$  is number of nearest neighbor bonds across the boundary per interfacial atom. The pair exchange energy required to calculate the interface Gibbs energies can be determined from the thermodynamics of the system by the CALPHAD method. For the Fe-W system, the chemical contribution to the heat of mixing of the bcc solid solution at equiatomic composition at the temperature 300 °C is assumed to be 2.5 kJ/g atom (see above). Using Becker's model we consider a representative (110) plane for a bcc structure, where there are 3/2 atoms per unit cell at the (110) plane.  $n_s$  can be calculated by considering the area of the (110) plane ( $=\sqrt{2}a_0^2$ ) and using an averaged lattice constant  $a_0=0.30158$  nm of the W and Fe structure [ $=3/2(1/\sqrt{2}a_0^2)$ ]. For the (110) interface there are two bonds per atom across the interface ( $Z_s=2$ ). The pair exchange energy per atom and per bond,  $\Omega$ , is calculated from the regular solid solution model by

$$\Omega = \frac{\Delta H_{\text{chem}}}{NnX_A X_B}, \quad (6)$$

where  $N$  is the Avogadro constant,  $n$  is number of nearest neighbor atoms ( $n=8$  for bcc structure), and  $X_A$  and  $X_B$  are the atomic fractions of components  $A$  and  $B$ , respectively.

We thus arrive at  $\Omega=2.1 \times 10^{-21}$  J for the bcc structure. Considering a concentration difference of two pure elements of  $\Delta c=1$  for interfaces between pure elements, the chemical contribution to the Fe/W interfacial energy amounts to  $\sigma_{\text{chem}}=0.05$  J/m<sup>2</sup>. Interfacial area  $S$  changes upon overall composition and size of domains. For the compositional dependence, the interfacial area  $S$  of unlike domains has a maximum value  $S_{\text{max}}$  at equiatomic composition for a certain domain size  $d$ . Therefore  $S$  is a function of composition and domain size  $d$ . If distribution of unlike domains is ordered and homogeneous, the area of interfaces amounts to  $S=2X_B S_{\text{max}}=2X_B 3/d$  (per unit volume), where  $X_B$  is the fraction of minority component, i.e.,  $X_B < 0.5$ . If  $X_B \geq 0.5$ , we have  $S=2X_A S_{\text{max}}$ . Physically,  $X_A$  is in the same manner as  $X_B$ .

The enthalpy related to the elastic strain of the coherent Fe/W interfaces is calculated based on Eq. (4) considering  $E=207$  GPa and 410 GPa for Fe and W, respectively, an average value of  $E$  (308 GPa) for the Fe/W interfaces is used. Thus the elastic contribution  $\Delta H_{\text{el}}$  due to the atomic mismatch at the Fe/W interfaces is derived to be 12.3 kJ/g atom for  $\epsilon=9.8\%$ . It is noted that there is no strain in both Fe and W components before milling. During milling the Fe and W components are deformed, the sizes become smaller and below a certain size, coherent interfaces are supposed to form. Simultaneously, strain arises from the coherent interface which is spread in the domains over a certain distance. The fraction of strained volume in the composite is estimated for cubic domains of size  $d$  and volume  $V_d=d^3$  by

$$\frac{\Delta V_d}{V_d} = \frac{3d^2 l}{d^3} = \frac{3l}{d}, \quad (7)$$

with  $l$  ( $\ll d$ ) being the length of strain region perpendicular to the coherent interfaces.  $l$  is assumed to be 1 nm, since in case of very large strain, misfit dislocations at the coherent interfaces will release part of the strain. Considering the concentration dependence of the interface area (see above) the elastic contribution to the excess enthalpy of the elemental composite can be expressed as

$$\Delta H_{\text{el}}^{\text{comp}} = \frac{\Delta V_d}{V_d} \frac{S}{S_{\text{max}}} \frac{1}{2} E \epsilon^2 \bar{V}_m. \quad (8)$$

On the basis of this model, the excess enthalpy of the composite is derived as

$$\Delta H^{\text{comp}} = \Delta H_{\text{chem}}^{\text{comp}} + \Delta H_{\text{el}}^{\text{comp}} = \frac{6X_B(\bar{V}_m \sigma_{\text{chem}} + l \Delta H_{\text{el}})}{d}. \quad (9)$$

$X_B$  is the fraction of minority component,  $X_A$  is in same manner as  $X_B$  as mentioned above. Then the critical size  $d_c$  of the domains below which the excess enthalpy exceeds the Gibbs energy of alloy formation,  $\Delta G_{\text{for}}$ , can be calculated by

$$d_c = \frac{6X_B(\bar{V}_m \sigma_{\text{chem}} + l \Delta H_{\text{el}})}{\Delta G_{\text{for}}}. \quad (10)$$

TABLE II. Calculation results of the chemical and elastic contributions to the coherent interfacial energy, the critical sizes of the domains for the formation of the different Fe-W phases, and the milling times required in the experiments.

Sample	Formed phase	$\Delta G_{\text{for}}$ (kJ/g at.)	$\Delta H_{\text{chem}}^{\text{comp}}$ (kJ/g at. %)	$\Delta H_{\text{el}}^{\text{comp}}$ (kJ/g at. %)	$d_c$ (nm)	Milling time (h)
Fe <sub>80</sub> W <sub>20</sub>	bcc	5.4	0.1	5.3	2.8	1400
Fe <sub>70</sub> W <sub>30</sub>	bcc	6.8	0.2	6.5	3.4	
	W+amor.	3.6	0.1	3.5	6.3	600
Fe <sub>50</sub> W <sub>50</sub>	bcc	7.1	0.3	6.8	5.4	
	W+amor.	2.5	0.1	2.4	15.3	50–100
Fe <sub>20</sub> W <sub>80</sub>	bcc	3.0	0.1	2.9	5.1	200

Table II gives calculation results of the critical sizes of the domains, the chemical and elastic contributions to the coherent interfacial energy for the formation of the different phases with respect to different compositions. It also gives the milling time to form these phases in the experiments. The values of the critical sizes amount to typically several nanometers and are in a reasonable microstructural range, supporting the proposed model. The critical sizes for the formation of different phases may explain why some phases are formed rapidly and some phases are formed sluggishly, e.g., the critical sizes of domains for the Fe<sub>20</sub>W<sub>80</sub> and the Fe<sub>80</sub>W<sub>20</sub> solid solutions are 5.1 and 2.8 nm, respectively, the milling times required in the experiments are 200 and 1400 h, respectively. Comparing the magnitudes of the chemical and elastic contributions, it can be concluded that the elastic strain that originates from the coherent interfaces plays the most important role in the phase formation of the Fe-W system by MA. In contrast, in the Cu-Co system which also exhibits positive heat of mixing for the solid solution, but has much smaller atomic size difference (1%), the large excess energy stored by MA mainly due to the chemical contribution of the coherent interfacial energy of Cu/Co domains.<sup>14</sup>

## V. SUMMARY AND CONCLUSIONS

The formation of amorphous phase is observed by mechanical alloying of elemental powder blenders in the Fe-W system for Fe-rich compositions. The thermodynamic analysis demonstrates that the Gibbs energy of the amorphous phase is lower than that of the bcc phase in the composition range from 17 to 42 at. % W ( $T=300^\circ\text{C}$ ), in agreement

with the experimental results, indicating that amorphization is thermodynamically favored in the Fe-W system, however the amorphous phase exhibits a positive heat of formation. A new model for amorphous phase formation in systems with positive heats of formation is proposed based on the development of coherent interfaces during mechanical alloying. The driving force for amorphous phase formation originates from the large elastic contribution to the excess enthalpy that arises from coherent interfaces between elemental components with different atomic sizes. The stored energy in the grain boundaries only plays a minor role. By comparing the results to those obtained in the Cu-Co system it can be concluded that for systems with small atomic size mismatch, the driving force primarily originates from the chemical contributions of coherent interfacial energy. In these cases, solid solutions are frequently formed by MA, as observed in the Co-Cu system. For systems with large atomic size mismatch, the elastic contribution plays an important role in energy storage by MA. In these cases formation of amorphous phases are energetically preferred with respect to the formation of a solid solution as observed in the Fe-W system.

## ACKNOWLEDGMENTS

One of the authors (H.Y.B.) is grateful to the financial support of the Alexander von Humboldt Foundation in Germany. Thanks also go to T. Klassen, R. Bohn, and W. Sinker for valuable discussions. The financial support of the Deutsche Forschungsgemeinschaft DFG-SP ‘‘Unterker Yhlte Metallschmelzen,’’ Az: Bo 691/5 is gratefully acknowledged.

\*Corresponding author. Email address: hybai@cl.cryo.ac.cn

<sup>1</sup>R. Bormann, in *Materials by Powder Technology, PTM 93*, edited by F. Aldinger (DGM Informationsgesellschaft, Oberursel, 1993), pp. 247–258.

<sup>2</sup>C. C. Koch, O. B. Cavin, C. G. McKamey, and J. O. Scarbrough, *Appl. Phys. Lett.* **43**, 1017 (1983).

<sup>3</sup>L. Schultz, *J. Less-Common Met.* **145**, 233 (1988).

<sup>4</sup>C. H. Lee, M. Mori, and U. Mizutani, *J. Non-Cryst. Solids* **117/118**, 733 (1990).

<sup>5</sup>E. Gaffet, C. Louison, M. Harmelin, and F. Faudot, *Mater. Sci. Eng., A* **134**, 1380 (1991).

<sup>6</sup>T. G. Richards and G. F. Johari, *Philos. Mag. B* **58**, 445 (1988).

<sup>7</sup>Y. Ogino, T. Yamasaki, S. Murayama, and R. Sakai, *J. Non-Cryst. Solids* **117/118**, 737 (1990).

<sup>8</sup>M. S. Boldrick, E. Yang, and C. N. J. Wagner, *J. Non-Cryst. Solids* **150**, 478 (1992).

<sup>9</sup>T. D. Shen, K. Y. Wang, M. X. Quan, and J. T. Wang, *J. Appl. Phys.* **71**, 1967 (1992).

<sup>10</sup>U. Mizutani and C. H. Lee, *Mater. Trans., JIM* **36**, 210 (1995).

<sup>11</sup>C. H. Lee, T. Fukunaga, Y. Yamada, and U. Mizutani, *J. Phase Equilib.* **14**, 167 (1993).

<sup>12</sup>C.-S. Xiong, Y.-H. Xiong, H. Zhu, and T.-F. Sun, *Nanostruct. Mater.* **5**, 425 (1995).

<sup>13</sup>A. R. Miedema, *Philips Tech. Rev.* **36**, 217 (1976).

- <sup>14</sup>C. Gente, M. Oehring, and R. Bormann, Phys. Rev. B **48**, 13244 (1995).
- <sup>15</sup>A. R. Yavari and P. J. Desre, Mater. Sci. Forum **88-90**, 43 (1992).
- <sup>16</sup>B. M. Clemens and T. C. Hufnagel, Appl. Phys. Lett. **69**, 2938 (1996).
- <sup>17</sup>G. K. Williamson and W. H. Hall, Acta Metall. **1**, 22 (1953).
- <sup>18</sup>Hai Yang Bai, C. Michaelsen, and R. Bormann, Phys. Rev. B **56**, R11361 (1997).
- <sup>19</sup>L. J. Swartzendruber, Bull. Alloy Phase Diagrams **3**, 161 (1982).
- <sup>20</sup>T. Takayama, M. Y. Wey, and T. Nishizawa, Trans. Jpn. Inst. Met. **22**, 315 (1981).
- <sup>21</sup>S. V. Nagender Naidu, A. M. Sriramamurthy, and P. Rama Rao, in *Phase Diagrams of Binary Iron Alloys*, Monograph Series on Alloy Phase Diagrams 9 (Fe), edited by H. Okamoto (American Society for Metals, Materials Park, OH, 1993), p. 444.
- <sup>22</sup>C. Michaelsen, C. Gente, and R. Bormann, J. Appl. Phys. **81**, 6024 (1997).
- <sup>23</sup>R. E. Watson and L. H. Bennett, Phys. Rev. Lett. **43**, 1130 (1979).
- <sup>24</sup>R. E. Watson and L. H. Bennett, CALPHAD: Comput. Coupling Phase Diagrams Thermochem. **5**, 25 (1980).
- <sup>25</sup>J. Friedel, Adv. Phys. **3**, 446 (1954).
- <sup>26</sup>D. J. Eshelby, J. Appl. Phys. **25**, 255 (1954).
- <sup>27</sup>C. Michaelsen, Philos. Mag. A **72**, 813 (1995).
- <sup>28</sup>B. Window, J. Appl. Phys. **63**, 1080 (1988).
- <sup>29</sup>G. Le Caër, P. Delcroix, T. D. Shen, and B. Malaman, Phys. Rev. B **54**, 12775 (1996).
- <sup>30</sup>C. Gente, Ph.D. thesis, 1996.
- <sup>31</sup>R. Becker, Ann. Phys. (Leipzig) **32**, 128 (1938).